Chapter 3

Decaying dark matter signal from different objects

In this Chapter we analyze dark matter distributions in several hundreds of dark matter-dominated objects in the local Universe (redshift $z < 0.3$) in order to estimate the dark matter decay map and determine optimal observational targets and detection strategy. We demonstrate that the expected dark matter decay signal (proportional to the "*dark matter column density*") increases slowly with the mass of the object. We determine a relation between the dark matter column density and the mass of the halo and demonstrate that the *scatter of this relation* can be predicted based on the existing numerical simulations of structure formation. Therefore, decaying dark matter would produce a unique all-sky signal, with a known slow-varying angular distribution — a signal that can be easily distinguished from any possible astrophysical background and therefore makes the astrophysical search for decaying dark matter an "almost direct" detection experiment.

3.1 Dark matter column density

The flux from the dark matter decay from a given direction (in $\mathrm{photons\ s^{-1}cm^{-2}}$) is given by

$$F_{\rm DM} = \frac{\Gamma E_\gamma}{m_{\rm DM}} \int_{\rm fov\ \mathit{cone}} \frac{\rho_{\rm DM}(\mathbf{r})}{4\pi |\mathbf{D}_L + \mathbf{r}|^2} \mathbf{dr}. \tag{3.1}$$

Here $\mathbf{D}_L$ is the *luminosity* distance between an observer and the centre of an observed object, $\rho_{\rm DM}(\mathbf{r})$ is the dark matter density, and the integration is

performed over the dark matter distribution inside the (truncated) cone – solid angle, spanned by the field of view (FoV) of the X-ray satellite. In case of distant objects[1], Eq. (3.1) can be simplified:

$$F_{\rm DM} = \frac{M_{\rm DM}^{\rm fov}\Gamma}{4\pi D_L^2}\frac{E_\gamma}{m_{\rm DM}}, \tag{3.2}$$

where $M_{\rm DM}^{\rm fov}$ is the mass of dark matter within a telescope field of view, $m_{\rm DM}$ – mass of the dark matter particle. In the case of small FoV, Eq. (3.2) simplifies to

$$F_{\rm DM} = \frac{\Gamma \mathcal{S}_{\rm DM}\Omega E_\gamma}{4\pi m_s}, \tag{3.3}$$

where

$$\mathcal{S}_{\rm DM} = \int_{l.o.s.} \rho_{\rm DM}(r)dr \tag{3.4}$$

is the *dark matter column density* (the integral goes along the line of sight), $\Omega \ll 1$ - FoV solid angle.

We start in Section 3.2 with the estimate of the decaying dark matter signal from the Milky Way halo. We demonstrate that unlike the case of annihilating dark matter, the decay signal is not concentrated in the Galactic Center (with its strong and uncertain astrophysical backgrounds), but varies slowly over the whole sky. In Sec. 3.3.2 we show that the dark matter column density weakly depends on properties of galaxies and galaxy clusters and changes no more than by an order of magnitude between the smallest galaxies and largest galaxy clusters. Finally, in Sec. 3.4 we discuss the obtained results.

3.2 Decay signal of the Milky Way halo

Because we reside in the inner part of Milky Way dark matter halo, it is the only object whose dark matter decay signal would be spread across the whole sky. The dark matter column density for the Milky Way halo is calculated using the expression [228]

$$\mathcal{S}_{\rm DM}^{MW}(\phi) = \int_0^\infty \rho_{\rm DM}\left(\sqrt{r_\odot^2 + z^2 - 2zr_\odot\cos\phi}\right)dz \tag{3.5}$$

[1]Namely, if luminosity distance D_L is much greater than the characteristic scale of the dark matter distribution.

where ϕ is the off-the-Galactic-center region, so that for the direction with galactic coordinates (l, b)

$$\cos\phi = \cos b \cos l. \tag{3.6}$$

and $r_\odot = 8\,\mathrm{kpc}$ is the distance from the Earth to the Sun.

It can be seen (e.g. [223, 228, 231]) that the function $S_{\rm DM}^{MW}$ can change only by a factor of few, when moving from the Galactic center ($\phi = 0^\circ$) to the anti-center ($\phi = 180^\circ$). That is, the Milky Way contribution to the decay is an all-sky signal. This is in stark contrast with the annihilating dark matter, where only few degrees around the Galactic Center represent a "region-of-interest".

3.3 Decaying dark matter signal from extragalactic objects

Let us now compare how contributions of other Galactic and extragalactic dark matter dominated objects compares with the column density of the Milky Way.

To properly compare the dark matter distributions in different objects, fitted by different density profiles, we *average* dark matter column density within a central part of an object. Namely, for each object we define a *characteristic radius* r_* (to be specified later, Sec. 3.3.2) and compute

$$\mathcal{S} = \frac{2}{r_*^2}\int_0^{r_*} r dr \int dz\, \rho_{\rm DM}(\sqrt{r^2+z^2}) \tag{3.7}$$

Integral over z extends to the virial boundary of a dark matter halo (and can be extended all the way to infinity, as the integral converges). The definition (3.7) implies that $\mathcal{S}$ is proportional to the dark matter surface density within r_* ($\mathcal{S} \propto \rho_* r_*$), where ρ_* is the average dark matter central density.

It has been argued for some time that ρ_* and r_* *for galaxies* are inversely proportional (for review see e.g. [247], see [248, 249] for recent results). Similar result, *extended to cluster scales*, was originally discussed in [223]. If this were true, the dark matter column density and hence expected signal would be the same for different objects.

To investigate this result and to study the distribution of dark matter column density in the objects in local Universe, we compile a catalog of more than 1000 dark matter density profiles of about 300 unique objects

Type	No. objects	References	Objects
Galaxy clusters	130	[250–262]	[263]
Galaxy groups	26	[198, 264, 265]	[266]
Elliptical galaxies	10	[267–271]	[272]
Spiral galaxies	180	[195, 273–300]	[301]
Dwarf spheroidals	11	[10, 192, 193, 196, 300, 302]	[303]
total	357		

Table 3.1: **Observational data.** The table lists the types of objects; total number of collected objects; references used to collect the observational data; and the final list of selected objects.

(see Table 3.1 for details). The dataset contains dark matter-dominated objects of all types, from dwarf spheroidal satellites of the Milky Way to galaxy clusters. It spans more than 8 orders of magnitude in the halo masses and more than four orders of magnitude in r_* ($0.2\,\mathrm{kpc} \lesssim r_* \lesssim 2.5\,\mathrm{Mpc}$). For each of the objects we compute the dark matter column density, averaging over several profiles (if different measurements for the same object are available).

3.3.1 Types of dark matter density profiles

The distribution of dark matter in galaxies, galaxy groups and galaxy clusters can be described by several density profiles. In this work we concentrated on four popular choices for dark matter density profiles and establish how their parameters are related to the characteristic radius, r_*.

I. Numerical (N-body) simulations of the cold dark matter model have shown that the dark matter distribution in all relaxed halos can be fitted with the universal Navarro-Frenk-White (NFW) profile [304, 305]:

$$\rho_{\mathrm{NFW}}(r) = \frac{\rho_s r_s}{r(1 + r/r_s)^2} \tag{3.8}$$

parametrised by ρ_s and r_s. A more useful parametrization is in terms of the halo mass, M_{200}, and the concentration parameter, $c \equiv R_{200}/r_s$. Namely, R_{200} is the radius at which the average dark matter density is 200 times larger than the critical density of the universe ρ_{crit}. The halo mass M_{200} is the total mass of dark matter within this radius. The variables (ρ_s,r_s) and

(M_{200}, c) are thus connected as follows:

$$\begin{aligned} \rho_s &= f(c)\rho_{\rm crit} \\ r_s &= \left(\frac{3M_{200}}{800\pi\rho_{\rm crit}c^3}\right)^{1/3} \\ f(c) &= \frac{200}{3}\frac{c^3}{\ln(c+1) - c/(c+1)} \end{aligned} \tag{3.9}$$

The equations (3.9) allow to determine $\mathcal{S} \propto r_s\rho_s$ (see Eq. 3.4 as a definition of column density), knowing halo mass and concentration parameter M_{200}, c.

II. The Burkert (BURK) profile [306] has been shown to be successful in explaining the kinematics of disk systems (e.g. [286]):

$$\rho_{\rm BURK}(r) = \frac{\rho_B r_B^3}{(r_B + r)(r_B^2 + r^2)}. \tag{3.10}$$

III. Another common parametrizations of cored profiles are given by the pseudo-isothermal (ISO) profile [287]

$$\rho_{\rm ISO}(r) = \frac{\rho_c}{1 + r^2/r_c^2}. \tag{3.11}$$

IV. Modified pseudo-isothermal (IS2) profile [296]

$$\rho_{\rm IS2}(r) = \frac{\rho_0}{(1 + r^2/r_0^2)^{3/2}}. \tag{3.12}$$

The quantity $\mathcal{S}(R)$ can be calculated analytically for all these choice of $\rho(r)$. For example, for the pseudo-isothermal profile one obtains:

$$\mathcal{S}_{\rm ISO}(R) = \frac{2\pi\rho_c r_c^2}{R^2}\left[\sqrt{R^2 + r_c^2} - r_c\right]. \tag{3.13}$$

For the NFW density distribution (3.8):

$$\mathcal{S}_{\rm NFW}(R) = \frac{4\rho_s r_s^3}{R^2}\left[\frac{\arctan\sqrt{R^2/r_s^2 - 1}}{\sqrt{R^2/r_s^2 - 1}} + \log\left(\frac{R}{2r_s}\right)\right]. \tag{3.14}$$

Notice, that this expression is real for both $R > r_s$ and $R < r_s$. The corresponding expression for the Burkert profile is rather lengthy and not very illuminating.

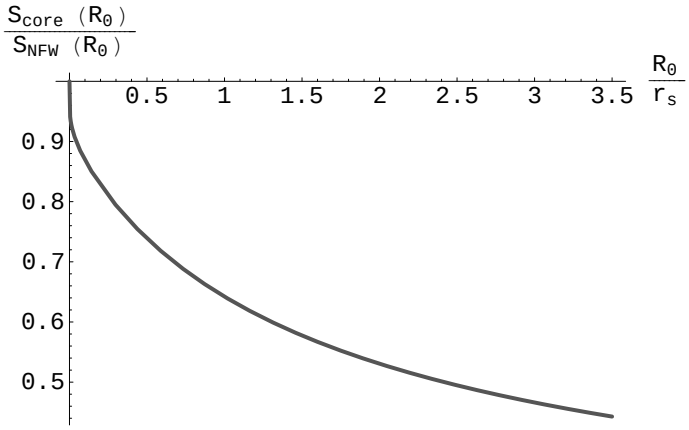

Figure 3.1: **The ratio of average column densities of the extreme cored and NFW profiles as a function of** R_0 (c.f. Eq. (3.15)).

3.3.2 Dependence of $\mathcal{S}$ on the inner slope of density profile.

In order to equally well fit the same rotation curve data, two dark matter profiles should have roughly the same mass within some radius R_0, determined by the observational data. If both profiles happen to have the same behaviour at large distances, their $\mathcal{S}$, averaged over R_0 will be essentially equal (as it is determined by the sum of the masses inside the sphere R_0 and in the outside of the cylinders, where the mass is dominated by the large r asymptotics).[2] In reality the situation is of course more complicated, one has to take into account the influence of baryons, the span of radii at which the data exists, etc.

We conservatively estimate the difference of column densities between a cusped and a cored profile as follows. We take the NFW density profile (3.8) as a representative of the cusped profile and its "extreme cored" counterpart $\rho_{core}(r)$ defined as follows:

$$\rho_{core}(r) = \begin{cases} \rho_{\rm NFW}(r), & r > R_0 \\ \rho_{\rm NFW}(R_0), & r \leq R_0 \end{cases} . \tag{3.15}$$

The column densities of these two profiles, averaged within R_0, differ only because the initial mass inside a *sphere* with radius R_0 for the cored pro-

[2] We will see below (Eq. (3.19)), that this is indeed the case for NFW and Burkert profiles.

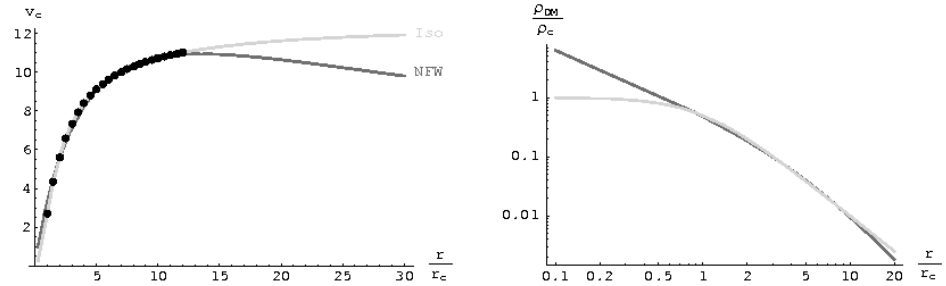

Figure 3.2: **Comparison of NFW and ISO profiles for the *simulated* rotation velocity points.** *Left panel:* the velocity data (black points, in units of $G_N \rho_c r_c^2$) is generated, assuming the ISO profile and fitted with the NFW profile. The parameters of the corresponding NFW profile (in the units of r_c, ρ_c) are given by eq. (3.16) in the text. *Right panel:* comparison of the density profiles with parameters, related by (3.16). The x-axis is in the units of isothermal core radius r_c.

file (3.15) diminishes as compared to the NFW case.

The resulting ratio of dark matter column densities is shown in the Supplementary Fig. 3.1 as a function of averaging radius R_0. In particular, for $R_0 = r_s$ this ratio is 64%, for $R_0 = 2r_s$ it equals to 53% and for $R_0 = 3r_s$ it drops to 47%. This implies that the difference of dark matter column densities between the cusped (NFW) and the extreme version of the cored profile (3.15) is within 50% for realistic averaging radii R_0 (usually $R_0 \sim 1-3r_s$). This difference is small compared to the intrinsic scatter expected on a object by object basis and well below the observational uncertainties on the parameters describing the density profile. This makes $\mathcal{S}$ a very robust quantity to compare observed properties of dark matter halos and results from numerical simulations and, consequently, test the prediction of the cold dark matter model.

The rotation curve of a galaxy is often fitted by several dark matter profiles (e.g. ISO and NFW). Let us analytically establish the relation between parameters of several profiles, *fitting the same rotation curve*. To this we take an ISO density profile and generate according to it the circular velocity profile $v_c^2(r)$, with r in the range $r_c \lesssim r \lesssim 15 r_c$.[3] Then we fit these data using an NFW profile (see Fig. 3.2, left). We find the following relations between

[3]The final result is not sensitive to the exact choice of this range.

the parameters of the two profiles:

$$\text{NFW vs. ISO} \quad : \quad r_s \simeq 6.1\, r_c \quad ; \quad \rho_s \simeq 0.11\, \rho_c \,. \tag{3.16}$$

The corresponding rotation curves and density profiles are shown in Supplementary Fig. 3.2.

Let us now compare the column densities for NFW and ISO profiles, whose parameters are related via Eq. (3.16). Results as a function of radius R are shown on Fig. 3.3. In particular, one sees that for $R = r_s$

$$\frac{\mathcal{S}_{\rm NFW}(r_s)}{\mathcal{S}_{\rm ISO}(6r_c)} \approx 0.91 \quad . \tag{3.17}$$

One may be surprised that the cusped profile leads to the smaller column density than the cored one (as Eq. (3.17) demonstrate). This result however, can be simply understood. We match the velocity profiles for the NFW and ISO at some off-center distances $R_0 \sim 2r_s$, by demanding that the mass inside this sphere is the same for both profiles. The ISO profile is shallower in the outer regions than the NFW one. The ratio between the mass inside a sphere of the radius R_0 and a cylinder with base radius R_0 is equal to 0.58 at $R_0 = 6r_c$ for ISO profile, while it is 0.63 at $R_0 = r_s$ for the NFW profile . Thus the mass in the outer part of a cylinder is larger for the shallower ISO profile than for the cuspy NFW one, which explains the result (3.17).

It is clear from previous considerations that $\mathcal{S}_{\rm NFW}$ and $\mathcal{S}_{\rm BURK}$ (similarly matched) should be essentially identical, as both profiles have identical behaviour at $r \to \infty$. Indeed, in the case of the NFW and Burkert profiles the relation between their characteristic parameters is given by

$$\text{NFW vs. BURK} \quad : \quad r_s \simeq 1.6 r_B \quad ; \quad \rho_s \simeq 0.37 \rho_B \tag{3.18}$$

which leads to

$$\frac{\mathcal{S}_{\rm NFW}(r_s)}{\mathcal{S}_{\rm BURK}(1.6r_s)} \approx 0.98 \quad . \tag{3.19}$$

Finally, it should be noticed that we assume an infinite extension for Dark Matter halos, when computing the column density. However, the integrals in (3.7) are convergent at large off-center distances and therefore the details of the truncation of the dark matter distributions for $R > R_{200}$ do not affect the value of $\mathcal{S}$ by more than 10%.

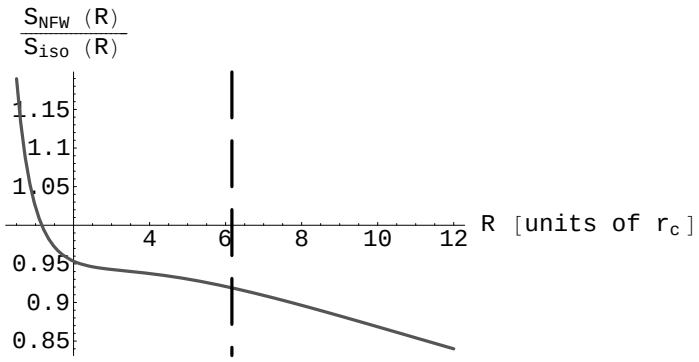

Figure 3.3: **Comparison of the column densities of NFW and ISO profiles.** Profiles describe the same data and their parameters are related via (3.16). The column density is averaged within various radii R. Dashed vertical line marks $R = r_s = 6.1 r_c$.

3.4 Universal properties of dark matter halos

The resulting dependence of dark matter column density on the type and mass of the objects is shown in Fig. 3.5.

By studying dark matter distribution in a large dataset of cosmic objects of different scale including dwarf, spiral and elliptical galaxies, galaxy groups and galaxy clusters we find the following relation between the characteristic dark matter column density $\mathcal{S}$ and the halo mass M_{halo} [4]:

$$\lg \mathcal{S} = 0.21 \lg \frac{M_{\rm halo}}{10^{10} M_\odot} + 1.79 \tag{3.20}$$

(with $\mathcal{S}$ in $M_\odot \ \mathrm{pc}^{-2}$).

To understand the relation (3.20) we compare our data with the results from cosmological N-body simulations within the ΛCDM [307, 308]. For each simulated halo we compute $M_{\rm halo}$, fit the particle distribution to the NFW density profile and calculate $\mathcal{S}$ using formula (3.7). The observational data together with results from ΛCDM numerical simulations [307] is plotted of the Fig. 3.5. The black dashed-dotted line on this Figure is the $\mathcal{S} - M_{\rm halo}$

[4] We use M_{200} as halo mass $M_{\rm halo}$. A proper definition of M_{200} can be found e.g. in [307] or in the Supplementary Information.

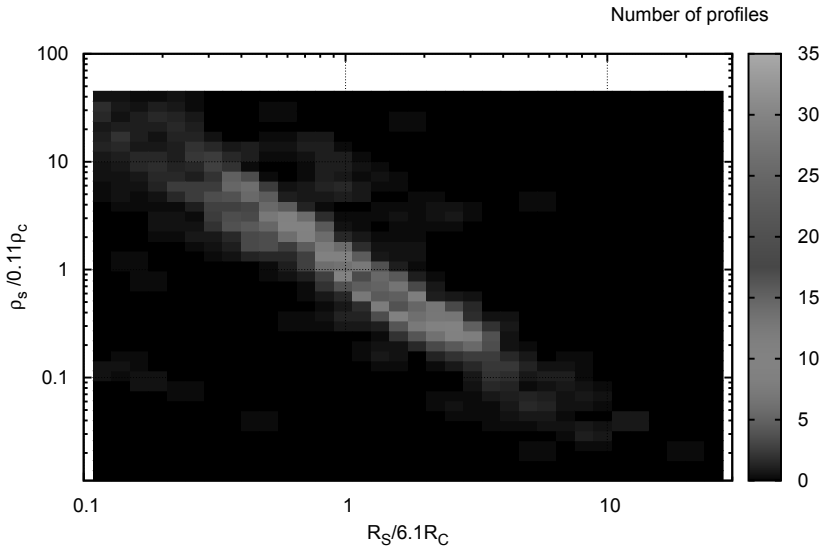

Figure 3.4: **Relation between parameters of NFW and ISO profiles in observed objects.** For objects for which both NFW and ISO fits of velocity rotation curves were available, we plot the ratios r_s/r_c and ρ_s/ρ_c. The maximum of the histogram lies in a region (3.16).

relation obtained from N-body simulations [307], using the fifth year cosmological parameters obtained from Wilkinson Microwave Anisotropy Probe (WMAP) satellite [309]. It fairly well reproduces the fit (3.20). Moreover, the pink shaded region (showing the 3σ scatter in the simulation data) contains most of the observational points within the halo mass range, probed by simulations. Therefore, the observed $M_{\rm halo} - \mathcal{S}$ scaling coincides with the relation between the parameters of dark matter density profiles observed in numerical simulations for long time [305, 307, 310] over more than five orders of magnitude in mass.

Dwarf spheroidal satellites (dSphs) of the Milky Way (orange diamonds on the Fig. 3.5) do not follow the relation (3.20). Recently the Aquarius project has produced a statistically significant sample of well resolved density profiles for satellite halos [308], making it possible to determine their $r_* - \rho_*$

relation. Satellites were found to be more concentrated than isolated halos and thus have a higher value of $\mathcal{S}$ at fixed $M_{\rm halo}$. Fig. 3.5 shows that the $\mathcal{S} - M_{\rm halo}$ relation for satellite halos (gray dashed line) from the Aquarius simulation [308] reproduces well the data on dSphs.

The fit to the data without the dSphs has the slope ≈ 0.23, much better quality of fit, and coincides extremely well with the results of N-body simulations [307] for isolated halos (black dashed-dotted line on Fig. 3.5). At masses below $10^{10} M_\odot$ no isolated halos were resolved in [307] and a simple toy model [307, 311] was used to predict the relation between parameters of NFW profile in a given cosmological scenario. The model (dotted line in the Fig. 3.5) fits well the results for the few spiral galaxies in this range. *Thus the agreement between observations and predictions from ΛCDM extend over more than eight orders of magnitude in mass*.

Comparison of our data with theoretical predictions (N-body simulations in our case) indicates that, despite the presence of various systematic errors in the data, the dark matter distributions in the observed objects exhibit a universal property – a systematic change of the average column density $\mathcal{S}$ as a function of the object mass ($\mathcal{S} \propto M_{\rm halo}^{0.2}$, relation (3.20)). This is different from the flat $\mathcal{S} = {\rm const}$ dependence, previously suggested [247–249]. The latter is based, in our view, on a confusion between the properties of isolated and non-isolated halos. Excellent agreement with pure dark matter simulations suggest also that the observed scaling dependence is insensitive to the presence of baryons, details of local environment, formation history.

The relation (3.20) can be used to search for deviations from cold dark matter model (e.g. warm dark matter models [105]) or modifications of gravity at large scales [312]. This motivates dedicated astronomical observations with all the data processed in a uniform way. Studies of the galaxies with the masses below $10^{10}\ M_\odot$ and galaxy clusters would be especially important.

Various scaling relations are known in astrophysics ("fundamental plane relation" for elliptical galaxies [313], "Tully-Fisher relation" for spiral galaxies [314], etc.). The relation (3.20) discussed in this Section differs in one crucial aspect: *it extends uniformly to all classes of objects at which dark matter is observed*. It would be very difficult to explain such a relation within Modified Newtonian dynamics [315] theory considered as an alternative to dark matter. That is why this relation, further confirmed, studied and understood analytically, may serve as one more evidence of the existence of dark matter.

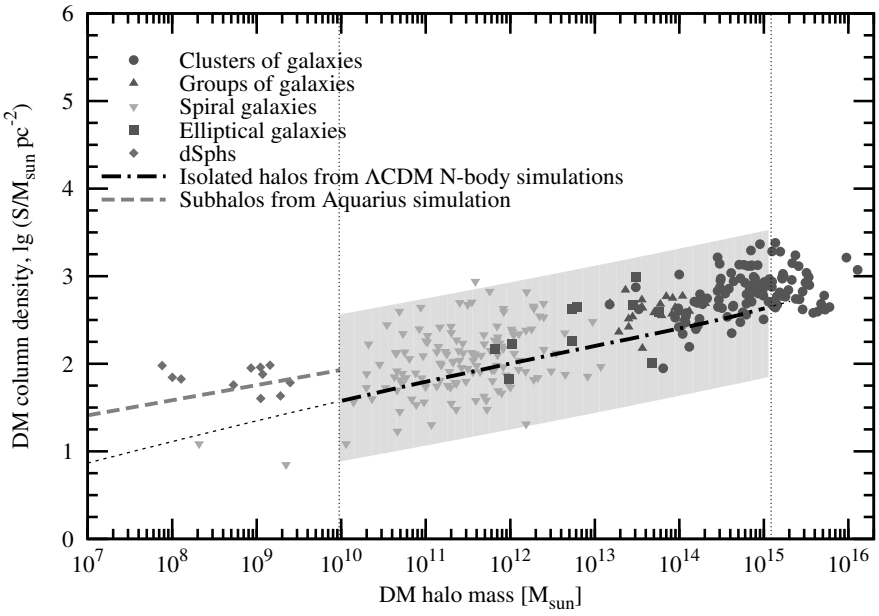

Figure 3.5: **Column density $\mathcal{S}$ as a function of halo mass $M_{\mathbf{halo}}$.** The black dashed-dotted line is the $S - M_{\rm halo}$ relation obtained from N-body simulations [307], using the WMAP fifth year cosmological parameters [309]. The shaded region shows the 3σ scatter in the simulation data. The vertical lines indicate the mass range probed by simulations. The dotted line is the theoretical prediction from the toy model for isolated halos [307, 311]. The gray dashed line showns the results from the Aquarius simulation for satellite halos [308].